Journal of Crystal Growth 314 (2011) 207–212

Contents lists available at ScienceDirect

Journal of Crystal Growth

journal homepage: www.elsevier.com/locate/jcrysgro

Studies on conventional and Sankaranarayanan–Ramasamy (SR) method grown ferroelectric glycine phosphite (GPI) single crystals

M. Senthil Pandian [a], N. Pattanaboonmee [b], P. Ramasamy [a,*], P. Manyum [b]

[a] Centre for Crystal Growth, SSN College of Engineering, Kalavakkam 603 110, Tamilnadu, India
[b] School of Physics, Institute of Science, Suranaree University of Technology, Nakhon Ratchasima, Muang 30000, Thailand

ARTICLE INFO

Article history:
Received 1 March 2010
Received in revised form
7 November 2010
Accepted 11 November 2010
Communicated by M. Fleck
Available online 18 November 2010

Keywords:
A1. Crystal morphology
A1. Defects
A1. Directional solidification
A1. X-ray diffraction
A2. Growth from solutions

ABSTRACT

Transparent single crystals of glycine phosphite were grown by Sankaranarayanan–Ramasamy (SR) method and conventional slow evaporation solution technique (SEST) which had the sizes of 100 mm in length, 30 mm diameter and $10\times11\times8$ mm^3. The conventional slow evaporation and Sankaranarayanan–Ramasamy method grown glycine phosphite single crystals were characterized using laser damage threshold, chemical etching, Vickers microhardness, UV–vis–NIR and dielectric analysis. The laser damage threshold value was higher in SR method grown GPI crystal as against conventional method grown crystal. The SR method grown GPI has higher hardness and also higher transmittance compared to conventional method grown crystal. The chemical etching and dielectric loss measurements indicate that the crystal grown by SR method has low density of defects and low value of dielectric loss compared to conventional method grown GPI crystal.

1. Introduction

Ferroelectric materials are widely used in various devices such as piezoelectric/electrostrictive transducers, pyroelectric infrared detectors (PIR), optical integrated circuits, optical data storage and display devices. Glycine phosphite (GPI) [$NH_2CH_2COOH\cdot H_3PO_3$], one of the ferroelectric compounds, crystallizes from its aqueous solution in the monoclinic system with space group P21/a at room temperature. Its cell parameters are $a=9.792$ Å, $b=8.487$ Å, $c=7.411$ Å; $\beta=100.43^\circ$. GPI undergoes a continuous ferroelectric–paraelectric phase transition at 224 K. Above the phase transition temperature, it belongs to the centrosymmetric point group 2/m and below the transition temperature, the spontaneous polarization arises along the monoclinic *b*-axis in its ferroelectric phase. GPI exhibits a low dielectric constant in all crystallographic directions [1] at the temperature range of 40 °C.

Conventional slow evaporation solution method grown GPI single crystal of dimension up to $30\times25\times20$ mm^3 and its morphology have been reported [2]. In conventional solution technique, many of the commonly observed characteristic growth induced defect structures comprising growth sector boundaries [3], liquid inclusions [3,4], growth band [5], slip band [6], low angle grain boundaries [7], dislocations [8], vacancies [8], cracks, stacking faults [9] and twins can be attributed to impurities. Growth bands are layers of varying impurity content and it is usually observed in solution grown crystals caused by fluctuations in the growth conditions [10] as well as growth sector boundaries [11]. It has also been observed that dislocations can originate from growth sector boundaries [12]. But in SR method grown crystals, we conclude that the defects of mother liquor inclusions, low angle grain boundaries, growth sector boundaries and dislocations are avoided. From this point of view, the Sankaranarayanan–Ramasamy (SR) method [13] was used to grow glycine phosphite (GPI) single crystal with a specific orientation in an ampoule.

In this paper we analyze conventional slow evaporation and ⟨0 1 0⟩ directed Sankaranarayanan–Ramasamy method grown GPI single crystals using laser damage threshold, chemical etching, Vickers microhardness, UV–vis–NIR and dielectric loss measurements. Standardized crystals with uniform thickness prepared with ⟨0 1 0⟩ orientation were used for laser damage threshold, chemical etching, Vickers microhardness, UV–vis–NIR, dielectric measurements and several samples were analyzed.

2. Crystal growth experiment

2.1. Synthesis and conventional growth

Glycine phosphite (GPI) was synthesized by dissolving equimolar ratio of GR grade glycine and phosphorous acid. Millipore

* Corresponding author. Tel.: +91 9283105760; fax: +91 44 27475166.
E-mail addresses: ramasamyp@ssn.edu.in, proframasamy@hotmail.com (P. Ramasamy).

0022-0248/$ - see front matter © 2010 Elsevier B.V. All rights reserved.
doi:10.1016/j.jcrysgro.2010.11.093

water of resistivity 18.2 MΩ cm was used as the solvent. The reaction is

$$NH_2CH_2COOH + H_3PO_3 \rightarrow NH_2CH_2COOH \cdot H_3PO_3$$

In order to get purified material, the synthesized GPI material was recrystallized several times before use for the growth. After 15 days good transparent hexagonal shaped single crystals of GPI were obtained with maximum dimension of $10 \times 11 \times 8$ mm^3 (Fig. 1(a)). The reported solubilities of GPI are ~42 g [14] and ~33 g [2] in 100 ml of water at 30 °C. So the solubility experiments were carried out using Millipore water as a solvent. Our measurement shows the solubility of GPI in 100 ml of water as 39 g at 30 °C. The crystal habit mainly consists of (0 1 0), (0 1 1), (0 0 1) and (2 1 1) faces [2,15].

2.2. SR method of crystal growth

A seed crystal of GPI was mounted at the bottom of the ampoule and the growth was carried out along the *b*-axis (〈0 1 0〉 orientation) (Fig. 1(a)). A ring heater of diameter 100 mm was placed around the top portion of the growth solution and a temperature of 40 °C with ±0.05 °C accuracy was set. This has provided a hot zone for achieving a uniform solvent evaporation. The bottom portion temperature was maintained at 34 °C for growing crystals.

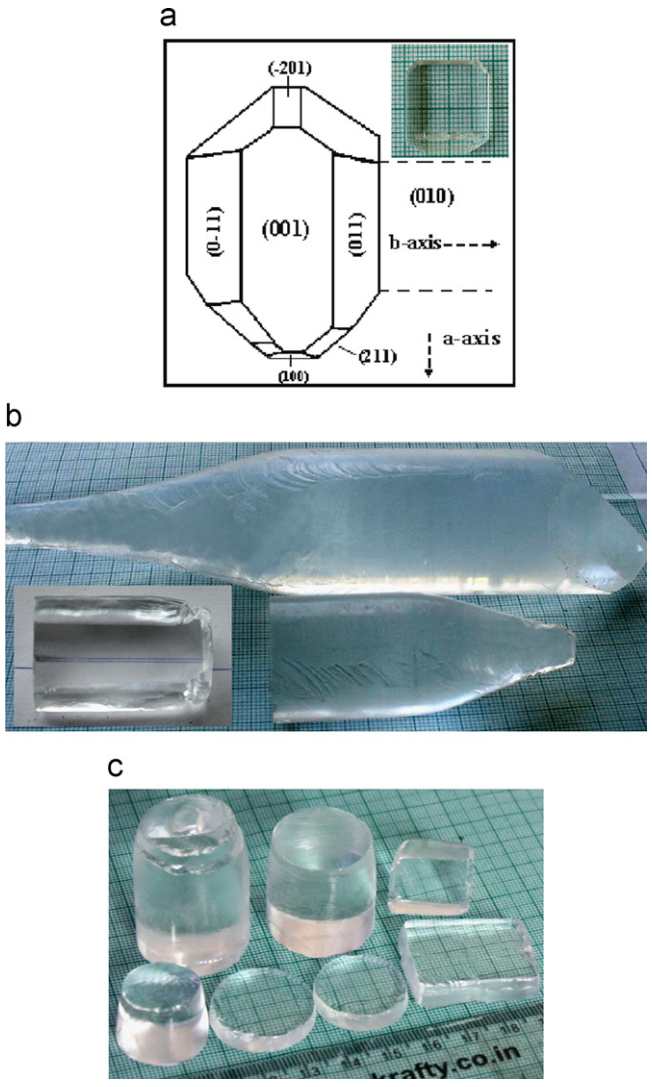

Fig. 1. (a) SEST grown GPI crystal and its Morphology, (b) Unidirectional 〈0 1 0〉 directed as grown GPI and Double refraction in GPI. (c) Cut and polished GPI ingots.

After 7 days, the seed crystal mounted at the bottom starts to grow. Under this growth condition, highly transparent crystal growth was seen and the growth parameters were kept constant for a long period for attaining continuous growth. The average growth rate was 2 mm/day. Transparent crystal of GPI (30 mm diameter and 100 mm length) was harvested within a period of 50 days (Fig. 1(b)).

Cut and polished SR grown GPI crystal with 20 mm thickness placed over a line on a page shows two distinct lines (Fig. 1(b)) like calcite and KAP crystals. This shows GPI crystal exhibits the birefringence effect and this behavior is used in birefringent crystal polarization devices [16]. The cut and polished GPI crystals are shown in Fig. 1(c).

3. Results and discussion

3.1. Single crystal X-ray diffraction

The single crystal XRD analysis of glycine phosphite (GPI) crystal was carried out using Enraf Nonius MACH3-CAT4 single crystal diffractometer with MoKα (λ=0.717 Å) radiation. The measured cell parameters were a=9.803 (6) Å, b=8.481 (2) Å, c=7.419 (2) Å; β=100.40°. The measured cell parameters are in good conformity with the published values [2,17].

3.2. Laser damage threshold (LDT)

Laser damage threshold analysis was made on the cut and polished SR method grown 〈0 1 0〉 directed GPI crystal of 3 mm thickness. Similarly in the conventional grown crystal a plate of 3 mm thickness in 〈0 1 0〉 direction was selected. Experimentally, a Q-switched diode array side pumped Nd:YAG laser operating at 532 nm radiation was used for the laser damage threshold studies. For this measurement 100 μm diameter of the beam was focused on the crystal with 8 cm focal length lens. In conventional method grown GPI crystal the average damage threshold was found to be 28 mJ/cm^2 for single shot mode. In the case of SR method, the LDT obtained on the GPI was 35 mJ/cm^2 (Fig. 2) and the observed results are given in Table 1. It shows that the GPI crystal grown by SR method has higher damage threshold than conventional method

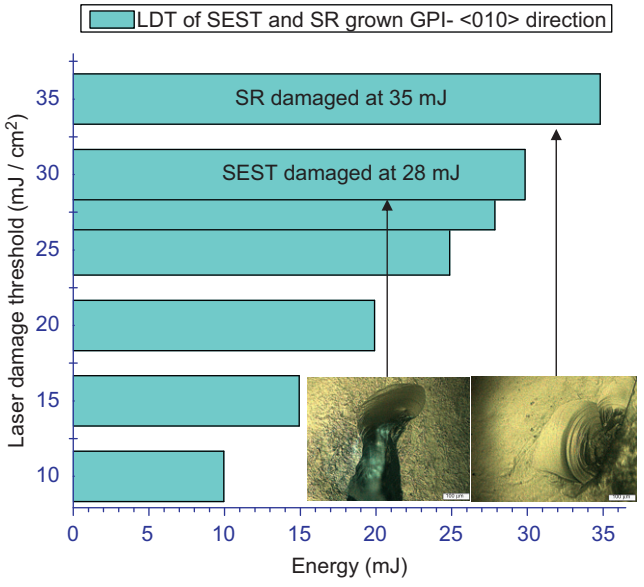

Fig. 2. Laser damage threshold values of conventional and SR method grown GPI crystals and its damaged patterns.

grown GPI. At the damage spot of SEST grown GPI crystal features like circular blobs, ring shape and cracks are seen (Fig. 2). Similar results observed in SR method grown GPI crystal are shown in Fig. 2.

The probable reasons for the lower laser damage threshold (LDT) of SEST method grown GPI crystals are inclusions and growth sector boundaries (GSB).

Solvent inclusions are potentially a major source of growth induced defects and it is very difficult to avoid the inclusion of solvent at the seed-crystal interface [10,18]. Inclusions are the main sources of dislocations and the generation of dislocations is strongly correlated with the formation of inclusions in the crystals. A variety of factors like, (i) variation in supersaturation of the solution, (ii) minor fluctuations in temperature during growth, (iii) non-uniform growth rates etc., govern the formation of inclusions. The presence of mother liquor inclusions in conventional method grown GPI crystal is shown in Fig. 3(a).

In SR method, the temperature gradient (at top 40 °C and bottom portion 34 °C) creates a concentration gradient along the growth ampoule, with a maximum and stable supersaturation at the bottom of the ampoule and all the solute molecules are directly approaching the ⟨0 1 0⟩ directed GPI crystal face and the surface attracts the atoms without any difficulty. Depending on the temperature at top and bottom portion the rate of evaporation of solvent is controlled effectively. For these reasons, in SR method grown GPI crystal there are (i) no growth fluctuation, (ii) uniform supersaturation near the surface of the crystal and (iii) stable growth rates, the dislocations of these three causes are avoided.

The SEST grown GPI crystals have different facets, growth sectors and growth sector boundaries. But in SR method, since the crystal is growing in selective growth orientation, the growth is on one facet only. There are no growth sector boundaries. Hence the dislocations associated with growth sector boundaries are absent in SR method grown GPI crystal.

Table 1
Comparison of laser damage threshold values of SEST and SR grown GPI crystal and its observations.

Test parameters				
Pulse width			7 ns	
Pulse rate			10 Hz	
Method	Laser pulses (Hz)	Energy (mJ)	Time (s)	Observation
SEST	1	10	5	No damage
		20	5	No damage
		27	5	Minor crack
		28	5	Damaged
	10	15	10	No damage
		20	10	No damage
		25	10	Slight damage
		27	10	Damaged
SR	1	5	5	No damage
		15	5	No damage
		25	5	No damage
		35	5	Damaged
	10	10	10	No damage
		20	10	No damage
		30	10	No damage
		34	10	Damaged

3.3. Chemical etching

The ⟨0 1 0⟩ direction of conventional and SR method grown GPI crystals were subjected to chemical etching and features were analyzed using a OLYMPUS U-TV0.5XC-3 optical microscope. The comparative study was made on both the method (SEST and SR) grown GPI crystals with water as an etchant. Inclusions are observed in conventional method grown GPI crystals (Fig. 3(a)) and this is normal in conventional solution grown crystals. The inclusions are of various shapes and sizes. Some of them are circular in shape and some appear like elongated circles. Low angle grain boundaries are clearly observed in SEST grown GPI crystal

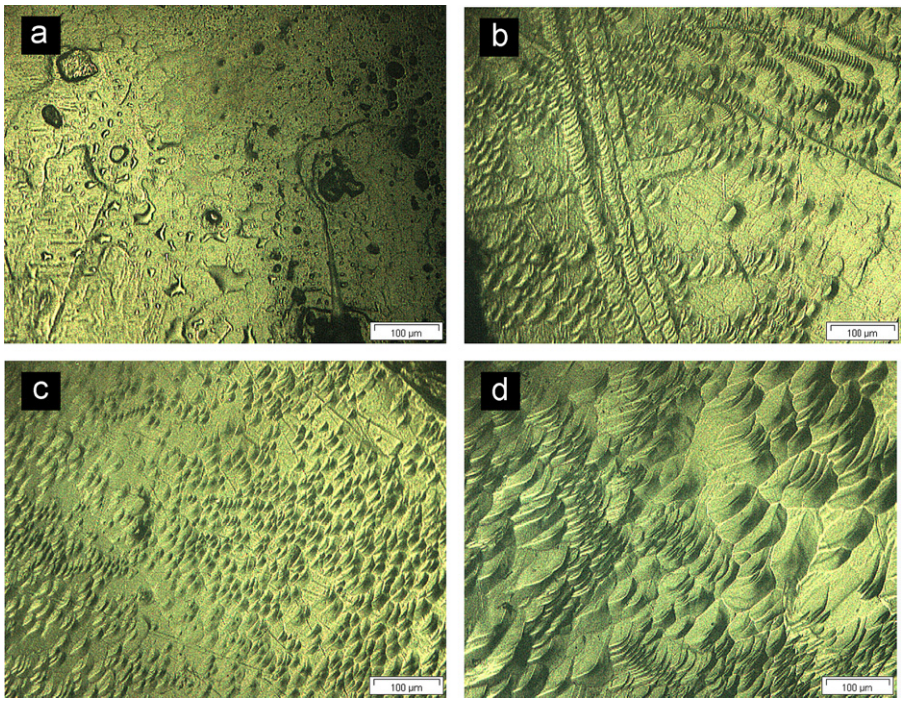

Fig. 3. (a) Microphotograph of inclusions and (b) Etch pattern around the low angle grain boundaries on SEST grown GPI crystal. (c) Etch pattern produced on the ⟨0 1 0⟩ direction of SEST grown GPI crystal by water after etching for 2 s. (d) Surface features observed on ⟨0 1 0⟩ directed SR grown GPI with water etchant for 2 s.

(Fig. 3(b)). Similar observations were reported on (1 0 0) cleavage of KCl crystals [7,19]. The segregation of impurities or the entrapment of solvent molecules at the boundaries during the growth process could be responsible for the observed low angle grain boundary [20].

Fig. 3(c) shows the etch pattern obtained on ⟨0 1 0⟩ direction of a SEST grown GPI crystal after etching with water for 2 s. Randomly distributed but strictly oriented etch pits are seen. The pits are distorted rectangular in shape. The estimated etch pit density (EPD) value of SEST grown GPI crystal was $9.25 \times 10^2/cm^2$.

Fig. 3(d) is an etch pit pattern of ⟨0 1 0⟩ directed SR method grown GPI crystal for 2 s with water etchant. Identical distorted rectangular shaped etch pits observed and compared to SEST grown GPI crystal with the same etching time of 2 s (Fig. 3(c)), the number of etch pits is less in SR method grown GPI crystal. The calculated etch pit density was $3.75 \times 10^2/cm^2$ (Fig. 3(d)).

In utilizing single crystals for any applications it is essential to grow single crystals containing a reduced dislocation density (DD). In conventional solution method, it is very difficult to grow crystals with low dislocation density, because dislocations are readily introduced during the growth process. There are two main sources of dislocations in conventional method grown crystals:

(i) Dislocations or other defects present in the seed crystal and
(ii) accidental nucleation during the growth process [21].

In SR method, the temperature gradient of top and bottom portion creates a concentration gradient along the glass ampoule, with a maximum supersaturation at the bottom of the ampoule and a minimum at the top of the ampoule. Therefore spurious nucleation along the length of the ampoule can be completely avoided. Low value of EPD indicates that SR method grown GPI crystal contains very low defects, which is in tune with high LDT.

3.4. Vickers microhardness

For a static indentation test, load '*P*' varying from 5 to 145 g was applied on the selected ⟨0 1 0⟩ direction on the GPI crystal over a fixed interval time of 15 s using Leitz-Wetzler microhardness tester. The Vickers microhardness value was calculated using the formula:

$$H_v = (1.854)P/d^2\ \mathrm{kg/mm^2}$$

where H_v is the Vickers hardness number (kg/mm^2), P is the applied load (g) and d is the average diagonal length (mm) of the indentation mark. A plot of the microhardness as a function of the applied load clearly indicates that hardness of the SEST and SR method grown GPI crystal increases with increase in load up to 70 g and having maximum hardness number at 70 g. In the present work, hardness number (H_v) was 56.3 kg/mm^2 for SEST grown GPI and 81.1 kg/mm^2 for SR method grown GPI crystal (Fig. 4(a)).

The presence of lattice defects influences many of the crystal properties, especially its mechanical strength. A qualitative explanation for the composition dependence of hardness is in terms of two contributions. One is lattice contribution and another one is due to the presence of defects like vacancies, impurity-vacancy pairs, dislocations, low angle grain boundaries [22]. It is already observed that the EPD of SEST grown GPI crystal is higher than the EPD of the crystal grown by SR method and the low angle grain boundaries are also present (Fig. 3(b)) in SEST grown GPI crystal. Lesser hardness value for conventional method grown crystals is due to entrapment of solvent inclusions during the growth process [23]. The liquid inclusion of GPI crystal observed in SEST method is shown in Fig. 3(a). But in SR method, there is no possibility to produce the inclusions in crystal. Hence higher hardness value for

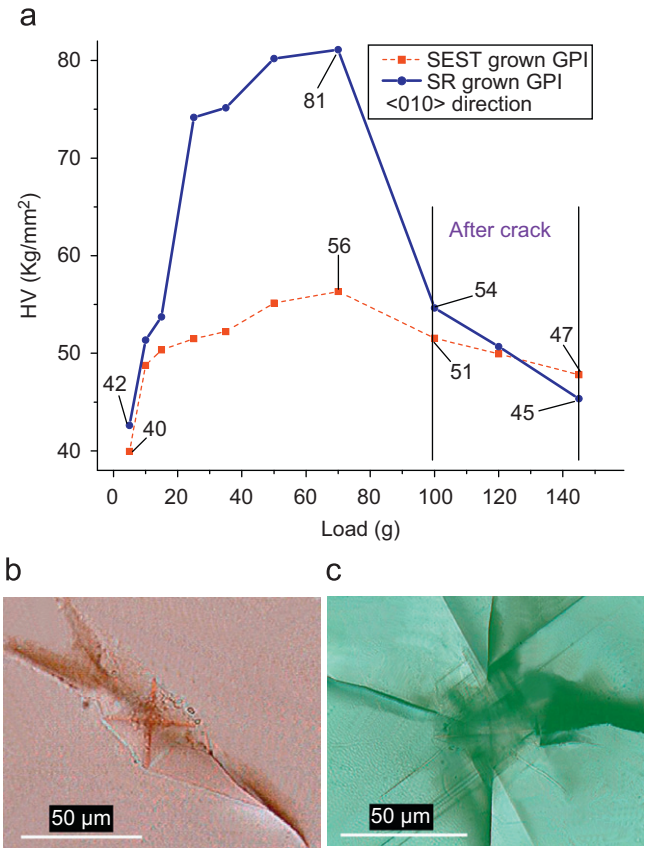

Fig. 4. (a) Vickers microhardness analysis. Indentation pattern of (b) conventional and (c) SR method grown GPI crystal at the load range of 100 g.

SR grown GPI crystal indicates greater stress required to form dislocation which confirms greater crystalline perfection.

Cracks begin to be formed for both the method (Conventional and SR) grown GPI crystals around the same load of 100 g, the influence of crack formation on hardness reduction was found to be higher for SR method grown GPI crystal. Cracks initiate above 100 g of load and tend to propagate with the increased load of 145 g, as evident from Fig. 4(b) and (c). It has been already reported that higher hardness crystals develop more cracks around the indentation mark [24]. This is the probable reason for higher reduction of hardness above 100 g of load in SR method grown GPI crystal.

The ratio between the load and size of indentation is given by Meyer's law as $P = ad^n$ where '*P*' is the load (g), '*d*' is the diameter of recovered indentation (mm), '*a*' and '*n*' are constants for a given material. According to Onitsch, $1.0 \le n \le 1.6$ for hard materials and $n \ge 1.6$ for soft materials [25]. The work hardening coefficient of conventional and SR grown GPI crystals are 1.5 and 1.3 (Fig. 5), respectively. Hence, it is suggested that GPI can be categorized as a hard material. Low value of work hardening coefficient (n) illustrates lesser defect [26] in the SR method grown GPI crystal since work hardening coefficient is caused by the dislocations present in the crystal.

3.5. UV–vis–NIR analysis

UV transmittance of the SEST and SR method grown GPI crystal was measured by Perkin-Elmer Lambda-35 spectrophotometer for the wavelength range 200–1100 nm with slit width 2 nm and scan speed 240 nm/min. Cut and polished SEST and SR grown ⟨0 1 0⟩ directed GPI crystals of 1 mm thickness were used. Fig. 6 shows the optical transmittance of about 58% and 66% for ⟨0 1 0⟩ oriented GPI crystals grown by SEST and SR method, respectively. The lower

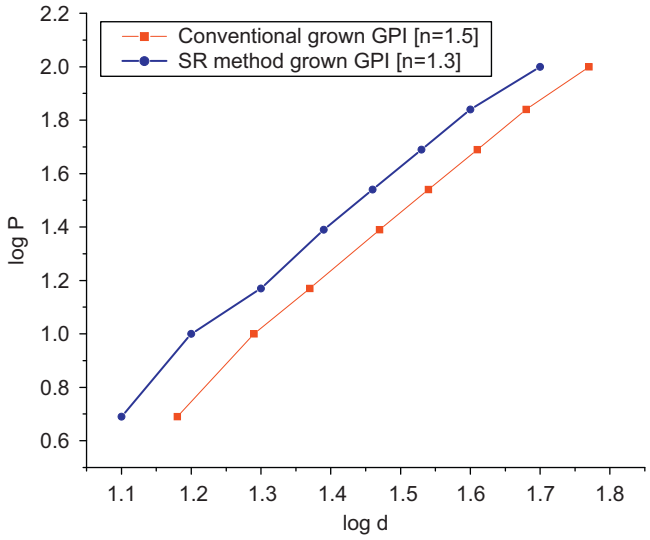

Fig. 5. Meyer's index of conventional and SR method grown GPI crystal.

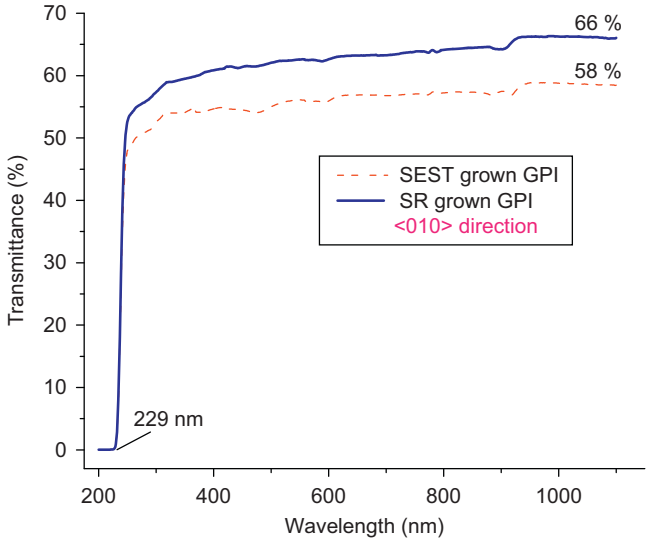

Fig. 6. UV–vis–NIR analysis.

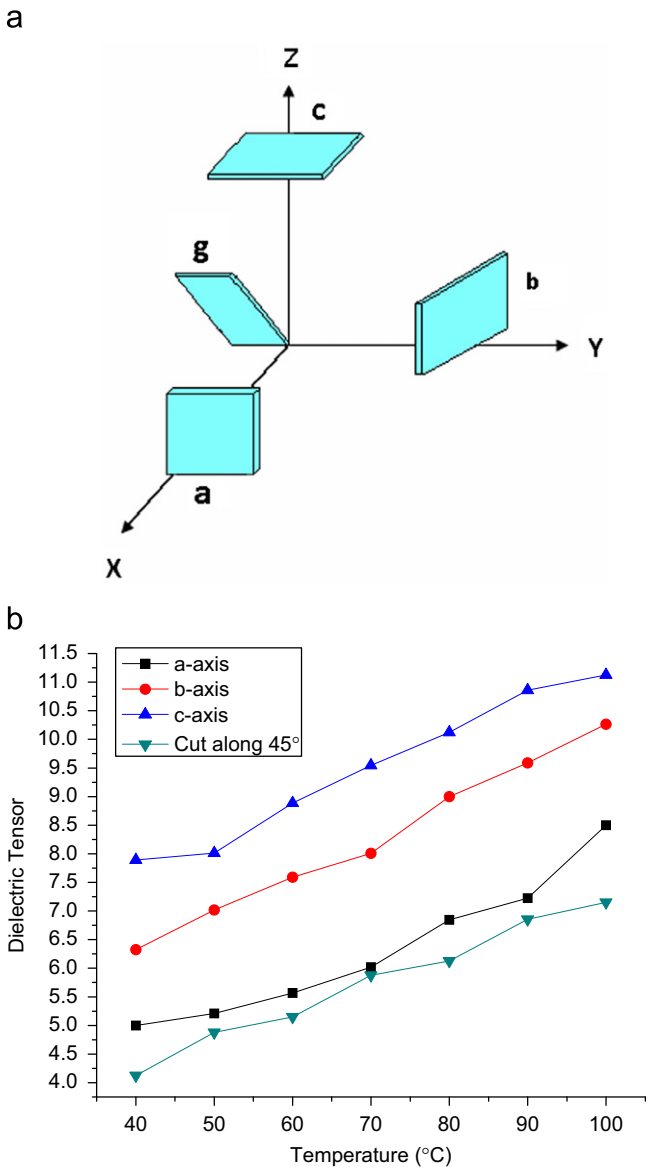

Fig. 7. (a) Samples for dielectric study and (b) Dielectric tensor components.

UV cutoff wavelength is around 229 nm. The UV transmittance of SR method grown GPI crystal is 8% higher than SEST grown GPI crystal. The enhancement in the percentage of transmission by 8% may be attributed to a reduced scattering from structural and crystallographic defects (point defects, line defects, low angle grain boundaries, vacancies or voids). The higher transmittance in SR grown GPI shows that the defect concentration in the grown crystal is less. The improvement of optical transparency of SR method grown TGS, KAP, ADP, KDP, DGZC, SA crystals has been reported [8,23,26–28].

3.6. *Dielectric analysis*

The dielectric measurement was carried out using the instrument Agilent 4284-A LCR meter. The method described in Ref. [29] was used to determine dielectric tensors. 1 mm thick plates were prepared from the SR method grown GPI crystal. Dielectric permittivities ε_{11}, ε_{22}, ε_{33} were determined from the *X*, *Y*, *Z* cut samples (Fig. 7(a)). ε_{13} was evaluated from Eq. (8) in Ref. [29]. The sample was electroded on either side with graphite coating to make it behave like a parallel plate capacitor. The dielectric permittivity of a crystalline material is a second rank tensor. For a monoclinic system there are four independent components. Anisotropy in the dielectric behavior has been observed. The dielectric tensor for GPI single crystal was determined as a function of temperature at 100 Hz frequency. The dielectric permittivity values vary with differently cut samples in the range 8.50–4.99 (a-cut), 10.26–6.32 (b-cut) and 11.12–7.89 (c-cut). The variations of dielectric permittivities are given in Fig. 7(b). The dielectric permittivity ε_{13} was obtained using the following formula:

$$\varepsilon'_{33} = \varepsilon_{11}\sin^2\theta + 2\varepsilon_{13}\sin\theta\cos\theta + \varepsilon_{33}\cos^2\theta$$

given in Ref. [29] where ε'_{33} dielectric permittivity for the sample g; ε_{11}—dielectric permittivity for the a-cut sample; ε_{33}—dielectric permittivity for the c-cut sample; $\theta = 45^\circ$. The dielectric permittivity ε_{13} is found to be -2.7. ε_{13} is negative indicating that the dielectric polarization occurs in the negative direction of the *Z*-axis when an electric field is applied along the positive direction of the *X*-axis [29].

The dielectric loss observations are made in the frequency range 100 Hz to 1 MHz at the temperature 40 °C. In conventional method grown GPI crystal, the dielectric loss has a high value of 1.3 at

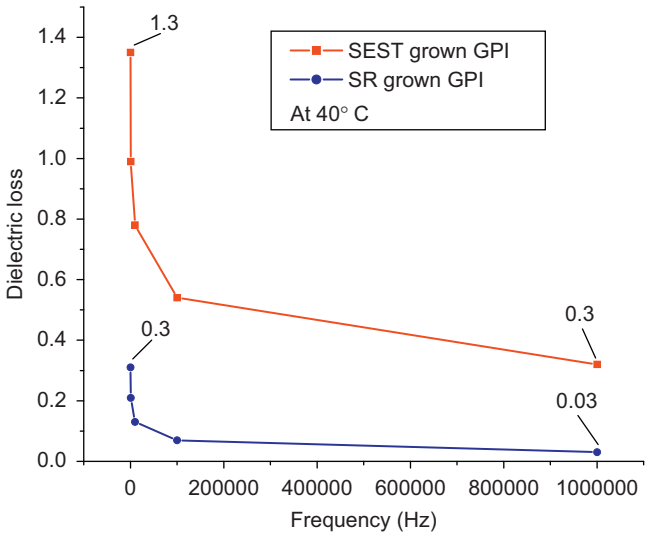

Fig. 8. Dielectric loss measurements of SEST and SR grown GPI crystal.

100 Hz and decreases to 0.3 at 1 MHz. But in the case of SR method grown GPI crystal the dielectric loss has a high value of 0.3 at 100 Hz and decreases to 0.03 at 1 MHz (Fig. 8). Low value of dielectric loss indicates that the SR grown GPI crystal contains minimum defects.

4. Conclusions

The high quality single crystal of glycine phosphite (GPI) was grown by Sankaranarayanan–Ramasamy (SR) method. A 30 mm diameter and 100 mm length GPI single crystal of orientation ⟨0 1 0⟩ was grown by this method. The higher laser damage threshold value indicates that SR method grown GPI crystal has high damage resistance.

Two main features have been observed from the etching experiments on SEST grown GPI crystal namely, inclusions and low angle grain boundaries. EPD is less in SR grown GPI crystal when compared to conventional method grown GPI crystal. The work hardening coefficient of SR and SEST grown GPI crystal was 1.3 and 1.5, respectively. It suggests that the GPI crystals grown by SR method have higher mechanical strength than SEST grown GPI crystal. The optical transparency of SR grown ⟨0 1 0⟩ directed GPI crystal is 8% higher than that of the crystal grown by conventional method. The four dielectric tensor components were measured and found to be $\varepsilon_{11}=8.50$, $\varepsilon_{22}=10.2$, $\varepsilon_{33}=11.1$, $\varepsilon_{13}=-2.7$. Low value of dielectric loss suggests that the SR grown GPI crystal possesses enhanced optical quality with low density of defects.

Acknowledgements

The authors would like to thank Dr. K. Venu Gopal Rao, ACRHEM, University of Hyderabad, for their support in laser damage threshold facilities, Prof. K. Kishan Rao, Kakatiya University, Warangal, for microhardness measurements, Dr. C.K. Mahadevan, S.T Hindu College, Nagercoil, for helping us in the dielectric measurements and Dr. S. Vijayan, Department of Mechanical engineering, SSN College of Engineering, for the help in taking photographs of etch patterns using optical microscope.

References

[1] E.V. Balashova, V.V. Lemanov, G.A. Pankova, Phys. Solid State 47 (2005) 183.
[2] A. Deepthy, H.L. Bhat, J. Cryst. Growth 226 (2001) 287.
[3] H.L. Bhat, R.I. Ristic, J.N. Sherwood, T. Shripathi, J. Cryst. Growth 121 (1992) 709.
[4] K. Kishnan Rao, V. Surender, Bull. Mater. Sci. 24 (2001) 665.
[5] I. Owczarek, K. Sangwal, J. Mater. Sci. Lett. 9 (1990) 440.
[6] M. Senthil Pandian, P. Ramasamy, J. Cryst. Growth 311 (2009) 944.
[7] A.R. Patel, R.M. Chaudhari, Indian J. Pure Appl. Phys. 7 (1969) 341.
[8] M. Senthil Pandian, N. Balamurugan, G. Bhagavannarayana, P. Ramasamy, J. Cryst. Growth 310 (2008) 4143.
[9] Suparna Sen Gupta, Tanusree Kar, Siba Prasad Sen Gupta, Jpn. J. Appl. Phys. 32 (1993) 1160.
[10] H.G. Gallagher, R.M. Vrcelj, J.N. Sherwood, J. Cryst. Growth 250 (2003) 486.
[11] H.L. Bhat, Prog. Cryst. Growth Charact. 11 (1985) 57.
[12] H.V. Alexandru, S. Antohe, J. Cryst. Growth 258 (2003) 149.
[13] K. Sankaranarayanan, P. Ramasamy, J. Cryst. Growth 280 (2005) 467.
[14] Jannatul Nayeem, Toshio Kikuta, Toshinari Yamazaki, Noriyuki Nakatani, Jpn. J. Appl. Phys. 39 (2000) 6612.
[15] Jannatul Nayeem, Hiroshi Wakabayashi, Toshio Kikuta, Toshinari Yamazaki, Noriyuki Nakatani, J. Korean Phys. Soc. 42 (2003) S1063.
[16] K. Buse, M. Luennemann, Phys. Rev. Lett. 85 (2000) 3385.
[17] S. Kalainathan, M. Beatrice Margaret, Mater. Sci. Eng. B 120 (2005) 190.
[18] Hugh G. Gallagher, Ranko M. Vrcelj, John N. Sherwood, J. Cryst. Growth 250 (2003) 486.
[19] K. Sangwal, G. Zaniewska, J. Mater. Sci. 19 (1984) 1131.
[20] N. Vijayan, G. Bhagavannarayana, Alex M.Z. Slawin, Mater. Lett. 62 (2008) 2480.
[21] V. Surender, Ph.D. Thesis, Department of Physics, Kakatiya University, 1994.
[22] U.V. Subba Rao, V.Hari Babu, Pramana 11 (1978) 149.
[23] M. Senthil Pandian, Urit Charoen In, P. Ramasamy, Prapun Manyum, M. Lenin, N. Balamurugan, J. Cryst. Growth 312 (2010) 397.
[24] K. Kishan Rao, V. Surender, B.Saritha Rani, Bull. Mater. Sci. 25 (2002) 641.
[25] Onitsch, E.M. Mikroscopia 2, 1947, p. 131.
[26] M. Senthil Pandian, P. Ramasamy, J. Cryst. Growth 312 (2010) 413.
[27] M. Senthil Pandian, N. Balamurugan, V. Ganesh, P.V. Raja Shekar, K. Kishan Rao, P. Ramasamy, Mater. Lett. 62 (2008) 3830.
[28] M. Senthil Pandian, P. Ramasamy, Proc. Solid State Phys. Symp. 54 (2009) 1115.
[29] Fapeng Yu, Shujun Zhang, Xian Zhao, Duorong Yuan, Chun-Ming Wang, Thomas R. Shrout, Cryst. Growth Des. 10 (2010) 1871–1877.